Gradient estimation for hexagonal grids and its application to classification of instrumentally registered tactile images

Stepan A. Nersisyan
Lomonosov Moscow State University
Faculty of Mechanics and Mathematics
Leninskie gory 1, 119991 Moscow
Russia
s.a.nersisyan@gmail.com

Vladimir M. Staroverov
Lomonosov Moscow State University
Faculty of Mechanics and Mathematics
Leninskie gory 1, 119991 Moscow
Russia
staroverovvl@yandex.ru

Abstract: **Introduction.** The majority of known finite difference schemes are designed for rectangular grids as rectangular grids are natural for many applications. However, these schemes are inapplicable to the analysis of images registered by Medical Tactile Endosurgical Complex (MTEC) — a novel device for intraoperative examination of tactile properties of tissues, as sensors of MTEC are located in nodes of a hexagonal grid.
Objectives. The aim of the research was to develop a finite difference scheme for gradient estimation designed for hexagonal grids, study theoretical properties of this scheme, and examine classification of MTEC-registered tactile images that included gradient estimation in its feature space.
Materials and Methods. Classification was tested using a library of artificial samples which contained six sample classes. Registration of tactile images was performed by 20 mm MTEC mechanoreceptors under five different angles which varied from 0° to 14°; 450 tactile images were registered in total. Classification algorithm utilized k-nearest neighbors classifier applied to a set of features associated with the most informative frame of a tactile image. Multiple stratified 5-fold cross-validation with 10 repeats was used for parameter optimization and measuring classifier accuracy.
Result. A finite difference scheme for gradient estimation on a hexagonal grid was constructed as a solution of a minimization problem directly related to the definition of differentiability. Error estimate for this scheme was obtained under C^2 assumption both for the case of error-free measurements of function values and for the case of measurements with errors. Classification of instrumentally registered tactile images that used gradient estimation space had mean accuracy above 90% for all classes of samples except one.
Conclusion. The designed finite difference scheme for gradient estimation on a hexagonal grid extends a list of mathematical methods applicable to an automated analysis of tactile images registered by MTEC. In particular, usage of feature space that includes gradient estimates increases the accuracy of multi-class classification of MTEC-registered tactile images.

Key–Words: Gradient estimation, Medical Tactile Endosurgical Complex, tactile image, k-nearest neighbors

1 Introduction

Gradient-based methods are widely used in processing of various types of data, including visual images and video streams [1, 2, 3, 4]. It was natural to hypothesize that these methods are also efficient for the analysis of instrumentally registered medical tactile images. Manual palpation, which is widely applied in open surgery, is inapplicable in minimally invasive surgery, including robot-assisted surgery [5, 6], and novel devices for instrumental registration of medical tactile images are being developed. While a number of devices for non-operative tactile examination exists [7, 8, 9], to the best of out knowledge the Medical Tactile Endosurgical Complex (MTEC) [10, 11, 12] is the only commercially available medical device for intraoperative instrumental palpation.

Currently results of intraoperative instrumental tactile examination performed with MTEC are reproduced visually in real time, and optionally a reproduction on a specially designed tactile display is performed [11, 12]. But the results are analyzed by a surgeon in fact with no support from any automated decision support system, which may be complicated in the initial segment of the learning curve and requires retaining of constant attention. Thus creating algorithms for automated analysis of instrumentally registered medical tactile images is a developing field with direct application in clinical medicine.

In [13] it was shown that in spite of low resolution of tactile images registered by MTEC both in

terms of a number of tactile pixels and a number of discretization levels, a successful automated classification of these images is possible by a combination of conventional machine learning methods with a specific feature set and a number of additional steps specially developed for MTEC-registered data analysis. Yet, in that study classification of tactile images was studied in case of nearly perfect angle in the tactile examination procedure, and it is known that deviation of a contact angle from 90° in MTEC-based tactile examination significantly affects the result [12]. In the present research we examined whether reliable classification of tactile images is still possible in case of essential deviations of the contact angle from 90° during examination. In particular, we tested classification reliability of k-nearest neighbors method applied for a feature space which includes gradient field of a selected tactile frame. As sensor of MTEC are located in the nodes of hexagonal grid, and standard finite-difference schemes are designed for rectangular grids, we developed a scheme for gradient estimation designed specifically for hexagonal grids.

The rest of the paper is organized as follows. In the *Materials and methods* section we give technical details related to the structure of tactile images, utilized library of tactile images and utilized classification approach. In the section *Gradient estimation on hexagonal grids* we present a finite-difference scheme for gradient estimation design for hexagonal grids and discuss properties of this scheme. Finally, in the section *Classification results* we evaluate reliability of automated classification of instrumental tactile images based on the combination of k-nearest method and a specific feature space which includes gradient characteristics.

2 Materials and methods

2.1 A structure of tactile images

In a MTEC-based tactile examination tactile images are registered by a tactile mechanoreceptor. Its operating head is equipped with pressure sensors located in nodes of a hexagonal grid. Sensors perform measurements 100 times per second and send measurement results to a computer which performs further processing. Thus, a tactile image consists of individual tactile frames containing values simultaneously registered by sensors. Each value after discretization is represented by a 8-bit integer, and the number of values in one frame is 7 for the mechanoreceptor with diameter 10 mm and 19 for the mechanoreceptor with diameter 20 mm. In the present research, similarly to [13], we used a library of tactile images registered by mechanoreceptors with 19 censors.

We note that tactile images registered during examinations of the same samples may differ essentially due to small shifts and rotations of a mechanoreceptor, differences in the pressing speed and force, differences in contact angles, etc.

2.2 A library of instrumentally registered tactile images

The study used a set of samples similar to the ones used in [13]. Specifically, the samples were made of a soft silicone (Shore hardness 00-10A) and had a shape of a rectangular box with size 40 mm $\times$ 35 mm $\times$ 10 mm. Samples belonged to one of six classes that differed in the hard embedment:

- *E-type*: samples without any embedments;
- *LF-type* and *LC-type*: samples with a spherical cap embedment with base diameter 8 mm and height 2.4 mm, oriented for tactile examination from the convex side and the flat side, respectively;
- *SF-type* and *SC-type*: samples similar to LF-type and LC-type but with different cap size (base diameter 4.7 mm and height 1.7 mm);
- *T-type*: samples with a horizontally oriented segment of a medical perfusion line (B. Braun Original Perfusion Line, diameter ca 2 mm) of length 20 mm.

The lot of manufactured samples contained at least 5 samples of each type. We performed 450 examinations of these samples with strictly controlled 5 different contact angles, i.e. totally 75 images per type (15 images for each contact angle). Contact angles had deviations from 90° equal to 0°, 3.6°, 7.1°, 10.6° and 14.0°.

2.3 Feature space and classifier type

First, for each tactile image we found *the most informative frame*, which was defined as the frame with maximum standard deviation of intraframe values. It allowed to reduce dimension and obtain certain invariance to some examination properties, e.g. pressing speed. Then we considered a series of frames forming a neighborhood of the most informative frame (with m_p and m_f frames preceding and following the most informative one, respectively) and for each sensor computed a mean over this series. This procedure can be treated as smoothing registered values over time axis, and taking the result of smoothing for

the time moment associated with the most informative frame. After that we performed scaling of resulting "smoothed" frame by dividing its values by their maximum (this scaling brought all values to $[0, 1]$ segment). Let f denote the result of these steps (i.e., f is smoothed and scaled most informative tactile frame).

Having f, we computed gradient $\nabla f = \left(\frac{\partial f}{\partial x}, \frac{\partial f}{\partial y}\right)^T$ as described in the section *Gradient estimation on hexagonal grids*.

Finally, for each of 19 sensors we computed standard deviation of values registered by this sensor in a tactile image and also scaled the result to $[0, 1]$ interval by dividing on the maximum standard deviation. N largest deviations were included to the features list.

Thus, $(57 + N)$-element vector was associated with each tactile image. This vector contained 19 values comprising smoothed and scaled most informative frame, 38 estimates of partial derivatives (19 estimates for each axis), and N largest scaled deviations.

In the resulting $(57 + N)$-dimensional feature space we we utilized k-nearest neighbor classifier [14, 15] for discriminating samples between six classes described above. The selection of k-nearest neighbors method was motivated by the results of the study [13]. Multiple stratified 5-fold cross-validation with 10 repeats was used for parameter optimization and measuring classifier accuracy.

In order to increase classification reliability, we used the trick described in [13]. Namely, for each tactile image from the training set we performed cloning by adding results of orthogonal transformations which map the sensor-associated hexagonal grid on itself. The transformations included rotation by angles multiple to 60° and symmetric reflections. Thus, for each tactile image we added 11 new images. The trick essentially improved classification quality.

3 Gradient estimation on hexagonal grids

In this section we present a final-difference scheme for estimating a gradient of a scalar field designed specially for hexagonal grids. We consider a real-valued differentiable function (scalar field) $f(x, y)$ defined in the closed regular hexagon G with center (x_0, y_0) and edge lengths h (Fig. 1) with known values in the center and vertices of G (see Fig. 1):

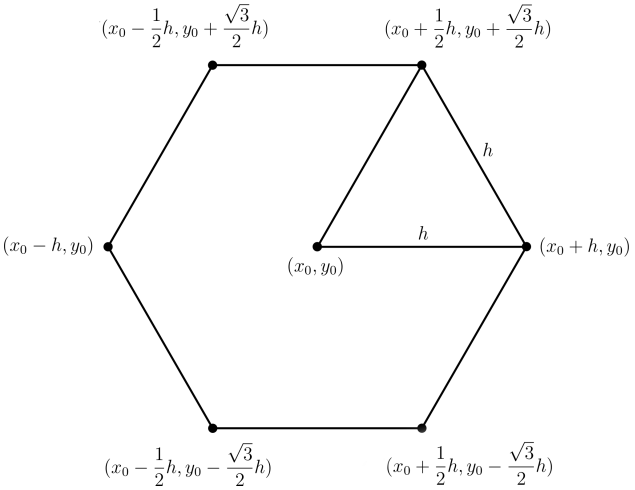

Figure 1: Regular hexagon with the center and vertices coordinates.

$$f_0 = f(x_0, y_0),$$
$$f_1 = f(x_0 + h, y_0),$$
$$f_2 = f(x_0 + \frac{1}{2}h, y_0 + \frac{\sqrt{3}}{2}h),$$
$$f_3 = f(x_0 - \frac{1}{2}h, y_0 + \frac{\sqrt{3}}{2}h),$$
$$f_4 = f(x_0 - h, y_0),$$
$$f_5 = f(x_0 - \frac{1}{2}h, y_0 - \frac{\sqrt{3}}{2}h),$$
$$f_6 = f(x_0 + \frac{1}{2}h, y_0 - \frac{\sqrt{3}}{2}h).$$

The aim is to estimate gradient of f in the point (x_0, y_0), i.e, to estimate

$$\nabla f\Big|_{(x_0,y_0)} = \left(\frac{\partial f}{\partial x}\Big|_{(x_0,y_0)}, \frac{\partial f}{\partial y}\Big|_{(x_0,y_0)}\right)^T =$$

$$= (f_x(x_0, y_0), f_y(x_0, y_0))^T,$$

based on the values f_i, $i \in \{0, 1, 2, 3, 4, 5, 6\}$.

As $f(x, y)$ is differentiable in the point (x_0, y_0),

$$f(x, y) = f(x_0, y_0) + f_x(x_0, y_0) \cdot (x - x_0) + \\ + f_y(x_0, y_0) \cdot (y - y_0) + o_{\|l\|\to 0}(\|l\|),$$

where (x, y) is an arbitrary point in G and $l = (x - x_0, y - y_0)^T$, $\|(x_1, \ldots, x_d)^T\| = \left(\sum_{i=1}^d x_i^2\right)^{\frac{1}{2}}$. Our approach is based on finding an estimate

$\Big(\hat{f}_x(x_0,y_0),\hat{f}_y(x_0,y_0)\Big)^T$ for $\nabla f\Big|_{(x_0,y_0)}$ which provides the best fit to the condition of differentiability for the vertices of G. That is, we consider the following optimization problem:

$$\left\|\begin{pmatrix}\frac{f_1-f_0}{h}\\ \frac{f_2-f_0}{h}\\ \frac{f_3-f_0}{h}\\ \frac{f_4-f_0}{h}\\ \frac{f_5-f_0}{h}\\ \frac{f_6-f_0}{h}\end{pmatrix}-\begin{pmatrix}1 & 0\\ \frac{1}{2} & \frac{\sqrt{3}}{2}\\ -\frac{1}{2} & \frac{\sqrt{3}}{2}\\ -1 & 0\\ -\frac{1}{2} & -\frac{\sqrt{3}}{2}\\ \frac{1}{2} & -\frac{\sqrt{3}}{2}\end{pmatrix}\times\begin{pmatrix}\hat{f}_x(x_0,y_0)\\ \hat{f}_y(x_0,y_0)\end{pmatrix}\right\|\longrightarrow$$

$$\longrightarrow \min_{\hat{f}_x,\hat{f}_y}.$$

The solution of the problem can be obtained by the conventional method of least squares [16]. The solution has the following form:

$$\hat{f}_x(x_0,y_0)=\frac{f_1-f_0}{3h}+\frac{f_2-f_0}{6h}+\frac{f_6-f_0}{6h}-$$
$$-\frac{f_4-f_0}{3h}-\frac{f_3-f_0}{6h}-\frac{f_5-f_0}{6h}=$$
$$=\frac{2f_1+f_2-f_3-2f_4-f_5+f_6}{6h}, \quad (1)$$

$$\hat{f}_y(x_0,y_0)=$$
$$=\frac{f_2-f_0}{2\sqrt{3}h}+\frac{f_3-f_0}{2\sqrt{3}h}\frac{f_5-f_0}{2\sqrt{3}h}-\frac{f_6-f_0}{2\sqrt{3}h}=$$
$$=\frac{f_2+f_3-f_5-f_6}{2\sqrt{3}h}. \quad (2)$$

The following theorem provides the error estimate for the presented scheme applicable for functions $f\in C^2(G)$.

Theorem 1 *Let $f(x,y)$ be twice continuously differentiable in G. Then for partial derivative estimates defined by formulas 1, 2 the following error estimates hold:*

$$\Big|\hat{f}_x(x_0,y_0)-f_x(x_0,y_0)\Big|<C_1Mh,$$
$$\Big|\hat{f}_y(x_0,y_0)-f_y(x_0,y_0)\Big|<C_2Mh.$$

Here C_1,C_2 are absolute constants, and

$$M=\max\Big\{\max_{\xi\in G}\Big|\frac{\partial^2 f}{\partial x^2}|_\xi\Big|,$$
$$\max_{\xi\in G}\Big|\frac{\partial^2 f}{\partial x\partial y}|_\xi\Big|,\max_{\xi\in G}\Big|\frac{\partial^2 f}{\partial y^2}|_\xi\Big|\Big\}.$$

Proof: The proof is based on the Taylor polynomial approximation of the function $f(x,y)$ with the Lagrange form of the remainder:

$$f(x,y)=f(x_0,y_0)+f_x(x_0,y_0)\cdot(x-x_0)+$$
$$+f_y(x_0,y_0)\cdot(y-y_0)+\frac{1}{2}d^2f|_\xi(x-x_0,y-y_0),$$

where $(x,y)\in G$, ξ is a point on two-dimensional interval from the point (x_0,y_0) to the point (x,y) and

$$d^2f|_\xi(\Delta x,\Delta y)=$$
$$=\frac{\partial^2 f}{\partial x^2}\Big|_\xi(\Delta x)^2+2\frac{\partial^2 f}{\partial x\partial y}\Big|_\xi\Delta x\Delta y+\frac{\partial^2 f}{\partial y^2}\Big|_\xi(\Delta y)^2.$$

Second differential can be trivially estimated in terms of M:

$$d^2f|_\xi(\Delta x,\Delta x)\le 4M(\Delta x)^2 \quad (\xi\in G).$$

Now let us proceed to the main computations:

$$\Big|\hat{f}_x(x_0,y_0)-f_x(x_0,y_0)\Big|=$$
$$=\Big|\frac{f_1-f_0}{3h}+\frac{f_2-f_0}{6h}+\frac{f_6-f_0}{6h}-$$
$$-\frac{f_4-f_0}{3h}-\frac{f_3-f_0}{6h}-\frac{f_5-f_0}{6h}-f_x(x_0,y_0)\Big|=$$
$$=\Big|\frac{1}{3}\Big(f_x(x_0,y_0)+\frac{1}{2h}d^2f|_{\xi_1}(h,0)\Big)-\frac{1}{3}f_x(x_0,y_0)+$$
$$+\frac{1}{6}\Big(\frac{1}{2}f_x(x_0,y_0)+\frac{\sqrt{3}}{2}f_y(x_0,y_0)+$$
$$+\frac{1}{2h}d^2f|_{\xi_2}(\frac{1}{2}h,\frac{\sqrt{3}}{2}h)\Big)-\frac{1}{12}f_x(x_0,y_0)-$$
$$-\frac{\sqrt{3}}{12}f_y(x_0,y_0)+\frac{1}{6}\Big(\frac{1}{2}f_x(x_0,y_0)-\frac{\sqrt{3}}{2}f_y(x_0,y_0)+$$
$$+\frac{1}{2h}d^2f|_{\xi_3}(\frac{1}{2}h,-\frac{\sqrt{3}}{2}h)\Big)-\frac{1}{12}f_x(x_0,y_0)+$$

$$+\frac{\sqrt{3}}{12}f_y(x_0,y_0)-\frac{1}{3}\Big(-f_x(x_0,y_0)+$$

$$+\frac{1}{h}d^2f|_{\xi_4}(-h,0)\Big)-\frac{1}{3}f_x(x_0,y_0)-$$

$$-\frac{1}{6}\Big(-\frac{1}{2}f_x(x_0,y_0)+\frac{\sqrt{3}}{2}f_y(x_0,y_0)+$$

$$+\frac{1}{2h}d^2f|_{\xi_5}(-\frac{1}{2}h,\frac{\sqrt{3}}{2}h)\Big)-\frac{1}{12}f_x(x_0,y_0)+$$

$$+\frac{\sqrt{3}}{12}f_y(x_0,y_0)-\frac{1}{6}\Big(-\frac{1}{2}f_x(x_0,y_0)-$$

$$-\frac{\sqrt{3}}{2}f_y(x_0,y_0)+\frac{1}{2h}d^2f|_{\xi_6}(-\frac{1}{2}h,-\frac{\sqrt{3}}{2}h)\Big)-$$

$$-\frac{1}{12}f_x(x_0,y_0)-\frac{\sqrt{3}}{12}f_y(x_0,y_0)\Big|\le$$

$$\le\frac{1}{6h}\Big(\Big|d^2f|_{\xi_1}(h,0))\Big|+\Big|d^2f|_{\xi_4}(-h,0))\Big|+$$

$$+\frac{1}{4}\Big(\Big|d^2f|_{\xi_2}(\frac{1}{2}h,\frac{\sqrt{3}}{2}h)\Big|+\Big|d^2f|_{\xi_3}(\frac{1}{2}h,-\frac{\sqrt{3}}{2}h)\Big|+$$

$$+\Big|d^2f|_{\xi_5}(-\frac{1}{2}h,\frac{\sqrt{3}}{2}h)\Big|+$$

$$+\Big|d^2f|_{\xi_6}(-\frac{1}{2}h,-\frac{\sqrt{3}}{2}h)\Big|\Big)\Big)\le 2Mh.$$

$$\Big|\hat{f}_y(x_0,y_0)-f_y(x_0,y_0)\Big|=\Big|\frac{f_2-f_0}{2\sqrt{3}h}+\frac{f_3-f_0}{2\sqrt{3}h}-$$

$$-\frac{f_5-f_0}{2\sqrt{3}h}-\frac{f_6-f_0}{2\sqrt{3}h}-f_y(x_0,y_0)\Big|=$$

$$=\frac{1}{2\sqrt{3}}\Big|\Big(\frac{1}{2}f_x(x_0,y_0)+\frac{\sqrt{3}}{2}f_y(x_0,y_0)+$$

$$+\frac{1}{2h}d^2f|_{\eta_1}(\frac{1}{2}h,\frac{\sqrt{3}}{2}h)\Big)-\frac{1}{2}f_x(x_0,y_0)-$$

$$-\frac{\sqrt{3}}{2}f_y(x_0,y_0)+\Big(-\frac{1}{2}f_x(x_0,y_0)+$$

$$+\frac{\sqrt{3}}{2}f_y(x_0,y_0)+\frac{1}{2h}d^2f|_{\eta_2}(-\frac{1}{2}h,\frac{\sqrt{3}}{2}h)\Big)+$$

$$+\frac{1}{2}f_x(x_0,y_0)-\frac{\sqrt{3}}{2}f_y(x_0,y_0)-$$

$$-\Big(-\frac{1}{2}f_x(x_0,y_0)-$$

$$-\frac{\sqrt{3}}{2}f_y(x_0,y_0)+\frac{1}{2h}d^2f|_{\eta_3}(-\frac{1}{2}h,-\frac{\sqrt{3}}{2}h)\Big)-$$

$$-\frac{1}{2}f_x(x_0,y_0)-\frac{\sqrt{3}}{2}f_y(x_0,y_0)-\Big(\frac{1}{2}f_x(x_0,y_0)-$$

$$-\frac{\sqrt{3}}{2}f_y(x_0,y_0)+\frac{1}{2h}d^2f|_{\eta_4}(\frac{1}{2}h,-\frac{\sqrt{3}}{2}h)\Big)+$$

$$+\frac{1}{2}f_x(x_0,y_0)-\frac{\sqrt{3}}{2}f_y(x_0,y_0)\Big|\le$$

$$\le\frac{1}{4\sqrt{3}h}\Big(\Big|d^2f|_{\eta_1}(\frac{1}{2}h,\frac{\sqrt{3}}{2}h)\Big|+$$

$$+\Big|d^2f|_{\eta_2}(-\frac{1}{2}h,\frac{\sqrt{3}}{2}h)\Big|+\Big|d^2f|_{\eta_3}(-\frac{1}{2}h,-\frac{\sqrt{3}}{2}h)\Big|+$$

$$+\Big|d^2f|_{\eta_4}(\frac{1}{2}h,-\frac{\sqrt{3}}{2}h)\Big|\Big)\le\frac{4M}{\sqrt{3}}h,$$

so the above error estimate holds with $C_1=2$ and $C_2=\frac{4}{\sqrt{3}}$.

□

Note that if we observe values $f_0,\dots,f_6$ with measurement error ε, i.e. we register values $\widetilde{f}_i$ which satisfy the inequalities $|\widetilde{f}_i-f_i|<\varepsilon$, the following form of the error estimate holds:

$$\Big|\hat{f}_x(x_0,y_0)-f_x(x_0,y_0)\Big|<C_1h+\frac{8\varepsilon}{3h},$$

$$\Big|\hat{f}_y(x_0,y_0)-f_y(x_0,y_0)\Big|<C_2h+\frac{8\varepsilon}{2\sqrt{3}h}.$$

These upper bounds illustrate that the scheme is applicable when measurement errors are present in case if the measurement error ε as essentially smaller than grid edge length h.

4 Classification results

Cross-validation showed that the optimal value for parameter k was 1 (which corresponds to simple nearest neighbor model), optimal metric was ℓ^1 (in this metric the distance between points $x=(x_1,\dots,x_d)$ and $y=(y_1,\dots,y_d)$ is defined as $\rho(x,y)=\sum_{i=1}^{d}|x_i-y_i|$), and optimal values for parameters m_p, m_f, N were 4, 7 and 4, respectively.

In order to compare the reliability of classification provided by the developed approach with the reliability of classification provided by the previously

developed classifier [13] we tested both method on the library of instrumentally registered tactile images described in the section *Materials and methods*. Parameters of the method from [13] were optimized for this library using the same cross-validation approach.

The main difference between two classifiers is in the feature spaces they use: the feature space for the proposed classifier includes estimates of gradient field, while feature space for the previously developed classifier includes only smoothed and scaled values of the most informative frame and largest scaled deviations of measurement results for individual sensors. There are also some additional minor differences between the classifiers in scaling of intraframe pressure values and measurement deviations.

Results of 5-fold cross-validation with 10 repeats are summarized in Fig. 2. Visually observable superiority of the proposed method is verified by the results of the statistical analysis: while no significant difference in classification reliability is observed for E-type, SC-type and T-type samples (cut-off 0.05), for the LF-type, LC-type and SF-type samples paired Wilcoxon signed-rank test resulted in p-values equal to $1.2 \times 10^{-2}, 1.3 \times 10^{-3}$ and 1.0×10^{-4}, respectively.

5 Conclusion

Automated analysis of instrumentally registered tactile images is a novel domain of applied mathematics which is motivated by advances in medical technologies and introduction of special purpose medical devices. In particular, MTEC allows intraoperative instrumental registration of tactile images in endoscopic surgery where conventional manual palpation is impossible.

A set of classical methods, such as k-nearest neighbors classification, have been shown to be efficient for the analysis of tactile images. Yet, specific properties of tactile images dictated by the hardware should be also taken into consideration. One of these properties is the geometry of sensors in the operating head of a MTEC mechanoreceptor, which is naturally associated with a hexagonal grid. The majority of known finite difference schemes are designed for rectangular grids and thus can not be applied to the analysis of MTEC-registered tactile images.

In this study we present a finite-difference scheme for estimating gradient field designed specifically for hexagonal grids. The scheme is constructed as a solution of a minimization problem directly related to the definition of differentiability. We discuss theoretical properties of this scheme, namely, error estimates both for the case of error-free measurements of function values and for the case of measurements with errors. We also show that usage of feature space that includes gradient estimates increases the accuracy of multi-class classification of MTEC-registered tactile images and provides reliable classification even in case of essential deviations of the contact angle from 90° during examination.

Acknowledgements: The authors thank Dr. Alexey V. Galatenko and Dr. Vladimir V. Galatenko for valuable comments and discussions. The research was supported by the Russian Science Foundation (project 16-11-00058 “The development of methods and algorithms for automated analysis of medical tactile information and classification of tactile images”).

References:

[1] F. Siegert, C. J. Weijer, A. Nomura and H. Mike, A gradient method for the quantitative analysis of cell movement and tissue flow and its application to the analysis of multicellular Dictyostelium development, *J. Cell. Sci.* 107, 2004, pp. 97–104.

[2] R. C. Gonzalez and R. E. Woods, *Digital image processing (4th edition)*, Pearson Prentice Hall, Upper Saddle River, New Jersey, 2007.

[3] A. Beck and M. Teboulle, Fast gradient-based algorithms for constrained total variation image denoising and deblurring problems, *IEEE Trans. Image Process.* 18(11), 2009, pp. 2419–2434.

[4] P. Bhat, C. L. Zitnick, M. Cohen and B. Curless, GradientShop: a gradient-domain optimization framework for image and video filtering, *ACM Trans. Graph.* 29(2), 2010, Article No. 10.

[5] H. M. Abdul-Muhsin and M. R. Humphreys, Advances in laparoscopic urologic surgery techniques, *F1000Res.* 5, 2016.

[6] A. M. Okamura, Haptic feedback in robot-assisted minimally invasive surgery, *Curr. Opin. Urol.* 19(1), 2009.

[7] V. Egorov V and A. P. Sarvazyan, Mechanical imaging of the breast, *IEEE Trans. Med. Imaging* 27(9), 2008, pp. 1275–1287.

[8] R. E. Weiss, V. Egorov, S. Ayrapetyan, N. Sarvazyan and A. Sarvazyan, Prostate mechanical imaging: a new method for prostate assessment, *Urology* 71(3), 2008, pp. 425–429.

[9] V. Egorov, H. van Raalte and V. Lucente, Quantifying vaginal tissue elasticity under normal and prolapse conditions by tactile imaging, *Int. Urogynecol. J.* 23(4), 2012, pp. 459–466.

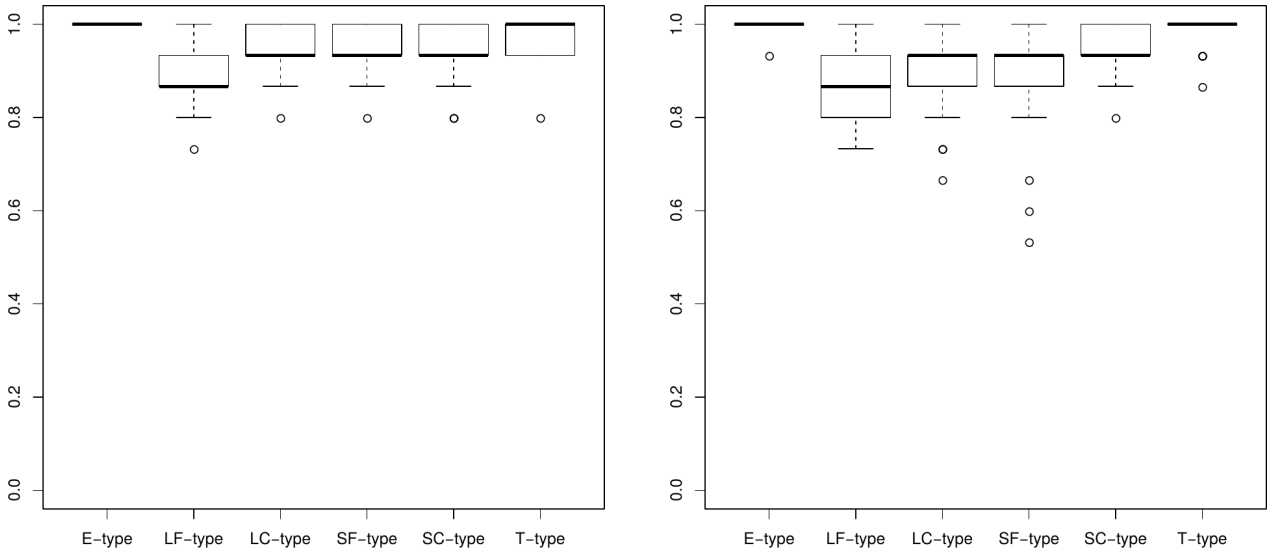

Figure 2: Boxplots of classification accuracy for 10 time repeated 5-fold cross-validation of classifiers with their optimal parameters. (a) The classifier with the gradient-based feature space. (b) The classifier without gradient-based features. Vertical axes indicate classification accuracy. The bottom and top of each box are the the lower and upper quartiles, and the band in each box is the median value.

[10] V. Barmin, V. Sadovnichy, M. Sokolov, O. Pikin and A. Amiraliev, An original device for intraoperative detection of small indeterminate nodules, *Eur. J. Cardiothorac Surg.* 46, 2014, pp. 1027–1031.

[11] R. F. Solodova, V. V. Galatenko, E. R. Nakashidze, I. L. Andreytsev, A. V. Galatenko, D. K. Senchik, V. M. Staroverov, V. E. Podolskii, M. E. Sokolov and V. A. Sadovnichy, Instrumental tactile diagnostics in robot-assisted surgery, *Med. Devices (Auckl)* 9, 2016, pp. 377–382.

[12] R. F. Solodova, V. V. Galatenko, E. R. Nakashidze, S. G. Shapovalyants, I. L. Andreytsev, M. E. Sokolov et al, Instrumental mechanoreceptoric palpation in gastrointestinal surgery, *Minim. invas. surg.*, 2017, Article ID 6481856.

[13] S. A. Nersisyan and Y. I. Rakhmatulin, Pattern recognition in low-resolution instrumental tactile imaging, *Int. J. Circ. Syst. Signal Pr.* 11, 2017, pp. 306–313.

[14] T. Cover and P. Hart, Nearest neighbor pattern classification, *IEEE Trans. Inf. Theory* 13(1), 1967, pp. 21–27.

[15] Z. Zhang, Introduction to machine learning: k-nearest neighbors, *Ann. Transl. Med.* 4(11), 2016, article 218.

[16] S. Margulies, Fitting experimental data using the method of least squares, *Rev. Sci. Instrum.* 39(4), 1968, pp. 478–480.